where the ω-integration is limited to the region $1/\tau_\varphi \leq |\omega| \leq kT/\hbar$. The averaged phase difference is seen to increase linearly in time:

$$\frac{1}{2} << (\varphi[\mathbf{x}_t^{cl}])^2 >_{ee}>_{imp} = \frac{t}{\tau_\varphi} \tag{11.152}$$

at a rate in accordance with the previous result for the phase-breaking rate, eq.(11.145).

The lack of effectiveness in destroying phase coherence by interactions with small energy transfers is reflected in the compensation at small frequencies between the two cosine terms appearing in the expression for the phase difference, eq.(11.149). In the case of diffusion-enhanced electron-electron interaction this compensation is crucial as there is an abundance of scattering events with small energy transfer, whereas the compensation was immaterial for electron-phonon interaction where the typical energy transfer is determined by the temperature.

Whereas the phase-breaking rate for electron-phonon interaction is model dependent, i.e., material dependent, we note the interesting feature that the phase-breaking rate for diffusion-enhanced electron-electron interaction is universal. In two dimensions we can rewrite

$$\frac{1}{\tau_\varphi} = \frac{e^2\sigma_0 kT}{2\pi\hbar^2} \ln\frac{k_F l}{2} . \tag{11.153}$$

Phase-breaking rates in accordance with eq.(11.145) have been extracted from numerous magnetoresistance measurements; confer for example references [58] and [59]. We note that at sufficiently low temperatures the electron-electron interaction dominates the phase-breaking rate in comparison with the electron-phonon interaction.

11.3.3 Temperature Dependence of Resistance

At finite temperature, the quantum correction to the dc conductance of a two-dimensional system is given by

$$\delta G(T) = -\frac{2D_0 e^2}{\hbar\pi} \int_0^{1/l} \frac{dQQ}{2\pi} \frac{1}{D_0 Q^2 + 1/\tau_\varphi} \tag{11.154}$$

The phase-breaking rate we have just shown has a power law dependence on the temperature

$$\frac{\hbar}{\tau_\varphi} = K\, T^p . \tag{11.155}$$

For the temperature dependence of the quantum correction to the conductance in the two-dimensional case we then obtain

$$\begin{aligned} \delta G(T) &= -\frac{e^2}{2\pi^2\hbar} \int_0^{1/l^2} dx \frac{1}{x + \frac{1}{D_0\tau_\varphi}} = -\frac{e^2}{2\pi^2\hbar} \ln\left(1 + \frac{\tau_\varphi}{2\tau}\right) \\ &\simeq -\frac{e^2}{2\pi^2\hbar} \ln\frac{D_0\tau_\varphi}{l^2} \end{aligned} \tag{11.156}$$

where we assume that the distance the electron diffuses before having inelastic scattering, the phase coherence length, $L_\varphi = \sqrt{D_0\tau_\varphi}$, satisfies

$$l \ll L_\varphi \ll L \tag{11.157}$$

where L is the size of the sample.

For the first quantum correction to the resistance we then have

$$\delta R(T) = -R_{cl}^2\, \delta G(T) \tag{11.158}$$

and obtain thereby the result for the temperature dependence of the resistance

$$\delta R(T) = -R_{cl}^2 \frac{e^2}{2\pi^2\hbar}\, p\, \ln\frac{T}{T_0} \tag{11.159}$$

where

$$T_0 = \left(\frac{D_0\hbar}{Kl^2}\right)^{1/p} . \tag{11.160}$$

Experimentally, the logarithmic temperature dependence was observed originally in reference [62]. In the relevant temperature regime of the experiment ($T \leq 1K$) the temperature T_0 is large, $T < T_0$, and it was found that in accordance with eq.(11.159), the resistance of a thin metallic film as a function of temperature increases with decreasing temperature. This effect of the temperature is due to the suppression of localization, thus diminishing the resistance value with increasing temperature. As the temperature increases, interference from large loops, $L \gg L_\varphi$, is destroyed by interactions. The coherent backscattering that inhibits the motion of the particle, is thus increasingly suppressed as the temperature increases, leading to the nonmetallic behavior of the conduction in thin metal films at low temperatures.

Varying the temperature, however, is not the proper diagnostic tool to uniquely reveal localization effects as diffusion-enhanced electron-electron interaction gives rise to similar temperature dependence of the resistance [52].

Exercise 11.1 *Find the weak-localization temperature dependence of the resistance in the three-dimensional case.*

11.4 Anomalous Magnetoresistance

From an experimental point of view, the disruption of coherence between time-reversed trajectories by an externally controlled magnetic field is the tool by which to study the weak-localization effect. Magnetoresistance measurements in

the weak-localization regime has considerably enhanced the available information regarding inelastic scattering times (and spin-flip and spin-orbit scattering times as discussed in section 11.6). The weak-localization effect thus plays an important diagnostic role in materials science.

The influence of a magnetic field on the Cooperon was established in section 11.2.1, and we have the Cooperon equation

$$\left\{-i\omega - D_0\{\nabla_{\mathbf{x}} - \frac{2ie}{\hbar}\mathbf{A}(\mathbf{x})\}^2 + 1/\tau_\varphi\right\} C_\omega(\mathbf{x},\mathbf{x}') \;=\; \frac{1}{\tau}\,\delta(\mathbf{x}-\mathbf{x}')\;. \qquad (11.161)$$

We can now safely study the dc conductivity, i.e., assume that the external electric field is static, so that its frequency is equal to zero, $\omega = 0$, as the Cooperon in an external magnetic field is no longer infrared divergent. The Cooperon is formally identical to the imaginary-time Schrödinger Green's function for a fictitious particle with mass equal to $\hbar/2D_0$ and charge $2e$ moving in a magnetic field (see exercise 2.2 on page 92). To solve the Cooperon equation for the magnetic field case, we can thus refer to the equivalent quantum mechanical problem of a particle in an external homogeneous magnetic field [13]. Considering the case of a homogeneous magnetic field,[33] and choosing the z-direction along the magnetic field and representing the vector potential in the Landau gauge, $\mathbf{A} = B\,(-y,0,0)$, the corresponding Hamiltonian is

$$\hat{H} \;=\; \frac{D_0}{\hbar}(\hat{p}_x + 2eB\hat{y})^2 \;+\; \frac{D_0}{\hbar}\left(\hat{p}_y^2 \;+\; \hat{p}_z^2\right)\;. \qquad (11.162)$$

The problem separates

$$\psi(x,y) \;=\; e^{\frac{i}{\hbar}p_x x}\, e^{\frac{i}{\hbar}p_z z}\,\chi(y) \qquad (11.163)$$

where the function χ satisfies the equation

$$-\frac{\hbar D_0}{2}\frac{d^2\chi(y)}{dy^2} \;+\; \frac{1}{2}\,\frac{\hbar}{2D_0}\,\tilde{\omega}_c^2\left(y - \frac{p_x}{2eB}\right)^2\chi(y) \;=\; \tilde{E}\,\chi(y) \qquad (11.164)$$

the shifted harmonic oscillator problem where $\tilde{\omega}_c$ is the *cyclotron* frequency for the fictitious particle, $\tilde{\omega}_c \equiv 4D_0|e|B/\hbar$, so that the energy spectrum is $E = \tilde{E} + \hbar D_0 Q_z^2 = \hbar\tilde{\omega}_c(n+1/2) + \hbar D_0 Q_z^2$, $n = 0,1,2,\ldots$; $Q_z = 2\pi n_z/L_z$, $n_z = 0,\pm1,\pm2,\ldots$. In the *particle in a magnetic field*-analog, n is the orbital quantum number and p_x the quantum number describing the position of the cyclotron orbit, and describes here the possible locations of closed loops. The Cooperon in the presence of a homogeneous magnetic field of strength B thus has the spectral representation

$$C_0(\mathbf{x},\mathbf{x}') \;=\; {\sum_{Q_z}}' \sum_{n=0}^{n_{max}} \int\frac{dp_x}{2\pi\hbar}\frac{\psi_{n,p_x}(\mathbf{x})\,\psi^*_{n,p_x}(\mathbf{x}')}{4D_0|e|B\tau\hbar^{-1}(n+1/2) + D_0\tau Q_z^2 + \tau/\tau_\varphi} \qquad (11.165)$$

where the ψ_{n,p_x} are the Landau wave functions

$$\psi_{n,p_x}(\mathbf{x}) \;=\; \frac{1}{\sqrt{L_z}}\, e^{\frac{i}{\hbar}p_x x}\, e^{iQ_z z}\,\chi_n(y - p_x/2eB)\;. \qquad (11.166)$$

[33] The case of an inhomogeneous magnetic field is treated in reference [63].

and $\chi_n(y)$ is the harmonic oscillator wave function. In accordance with the derivation of the Cooperon equation, we can only describe variations on length scales larger than the mean free path. The sum over the *orbital*-quantum number n should therefore terminate when $D_0\tau|e|Bn_{max} \sim \hbar$, i.e., at values of the order of $n_{max} \simeq l_B^2/l^2$, where $l_B \equiv (\hbar/|e|B)^{1/2}$ is the magnetic length.

To calculate the Cooperon for equal spatial values, $C_0(\mathbf{x},\mathbf{x})$, we actually do not need all the information contained in eq.(11.165), since by normalization of the wave functions in the completeness relation we have

$$\int_{-\infty}^{\infty}\frac{dp_x}{2\pi\hbar}\,\chi_n^*\left(y - \frac{p_x}{2eB}\right)\chi_n\left(y - \frac{p_x}{2eB}\right) \;=\; -\frac{2eB}{2\pi\hbar}\int_{-\infty}^{\infty}dy\,|\chi_n(y)|^2 \;=\; -\frac{2eB}{2\pi\hbar} \qquad (11.167)$$

and thereby

$$C_0(\mathbf{x},\mathbf{x}) \;=\; -\frac{2eB}{2\pi\hbar}{\sum_{Q_z}}'\sum_{n=0}^{n_{max}}\frac{1}{4D_0|e|B\tau\hbar^{-1}(n+1/2) + D_0\tau Q_z^2 + \tau/\tau_\varphi}\;. \qquad (11.168)$$

11.4.1 Magnetoresistance in Thin Films

We now consider the magnetoresistance of a film of thickness a, choosing the direction of the magnetic field perpendicular to the film.[34] Provided the thickness of the film is smaller than the phase coherence length, $a \ll L_\varphi$ (the thin film, or quasi-two-dimensional criterion), or the usually much weaker restriction that it is smaller than the magnetic length, $a \ll l_B$, only the smallest value of $Q_z = 2\pi\,n/L_z$, $n = 0,\pm1,\pm2,\ldots$ contributes to the sum. Since the smallest value is $Q_z = 0$, we obtain, according to eq.(11.13), for the quantum correction to the conductivity

$$\delta\sigma(B) \;=\; \frac{e^3 B D_0\tau}{\pi^2\hbar^2 a}\sum_{n=0}^{n_{max}}\frac{1}{4D_0|e|B\tau\hbar^{-1}(n+1/2) + \tau/\tau_\varphi}\;. \qquad (11.169)$$

Employing the property of the di-gamma-function ψ (see for example reference [64])

$$\psi(x+n) \;=\; \psi(x) \;+\; \sum_{n=0}^{n-1}\frac{1}{x+n} \qquad (11.170)$$

we get for the magnetoconductance

$$\delta G_{\alpha\beta}(B) \;=\; \frac{e^2}{4\pi^2\hbar}\,\tilde{f}_2(4D_0|e|B\hbar^{-1}\tau_\varphi)\,\delta_{\alpha\beta} \qquad (11.171)$$

where

$$\tilde{f}_2(x) \;=\; \psi\left(\frac{1}{2} + \frac{1}{x}\right) \;+\; \psi\left(\frac{3}{2} + n_{max} + \frac{1}{x}\right)\;. \qquad (11.172)$$

[34] The strictly two-dimensional case can also be realized experimentally, for example by using the two-dimensional electron gas accumulating in the inversion layer in a MOSFET or heterostructure.

The magnetoconductance of a thin film is now obtained by subtracting the zero field conductance. In the limit $B \to 0$, the sum can be estimated to become

$$\sum_{n=0}^{n_{max}} \frac{1}{4D_0|e|B\tau\hbar^{-1}(n+1/2)+\tau/\tau_\varphi} \quad \to \quad \ln(n_{max} 4D_0|e|B\hbar^{-1}\tau_\varphi)\,. \tag{11.173}$$

Using the property of the di-gamma-function

$$\lim_{n\to\infty} \psi\left(\frac{3}{2}+n+\frac{1}{x}\right) \;\simeq\; \ln n \tag{11.174}$$

we finally arrive at the low-field magnetoconductance of a thin film

$$\Delta G_{\alpha\beta}(B) \;\equiv\; \delta G_{\alpha\beta}(B) - \delta G_{\alpha\beta}(B\to 0) \;=\; \frac{e^2}{2\pi^2\hbar}\, f_2(B/B_\varphi)\, \delta_{\alpha\beta} \tag{11.175}$$

where

$$f_2(x) \;=\; \ln x \;+\; \psi\left(\frac{1}{2}+\frac{1}{x}\right) \tag{11.176}$$

and $B_\varphi = \hbar/4D_0|e|\tau_\varphi$, the (temperature-dependent) characteristic scale of the magnetic field for the weak-localization effect, is determined by the inelastic scattering. This scale is indeed small compared to the scale for classical magnetoresistance effects $B_{cl} \sim m/|e|\tau$, as $B_\varphi \sim B_{cl}\,\hbar/\epsilon_F\tau_\varphi$.[35] The weak-localization magnetoconductance is seen to be sensitive to very small magnetic fields, namely when the magnetic length becomes comparable to the phase coherence length, $l_B \sim L_\varphi$, or equivalently, $\omega_c\tau \sim \hbar/\epsilon_F\tau_\varphi$. Since the impurity mean free time, τ, can be much smaller than the phase coherence time τ_φ, the above description can be valid over a wide magnetic field range where classical magnetoconductance effects are absent. Classical magnetoconductance effects are governed by the orbit bending scale, $\omega_c\tau \sim 1$, whereas the weak-localization quantum effect sets in when a loop of typical area L_φ^2 encloses a flux quantum.[36] We note the limiting behavior of the function

$$f_2(x) \;=\; \begin{cases} \frac{x^2}{24} & \text{for} \quad x \ll 1 \\ \\ \ln x & \text{for} \quad x \gg 1\ . \end{cases} \tag{11.177}$$

The magnetoconductance is positive, and seen to have a quadratic upturn at low fields, and saturates beyond the characteristic field in a universal fashion, i.e.,

[35] In terms of the mass of the electron we have for the mass of the fictitious particle $\hbar/2D_0 \sim m\hbar/\epsilon_F\tau$, and the low magnetic field sensitivity can be viewed as due to the smallness of the fictitious mass in the problem.

[36] Beyond the low-field limit, $\omega_c\tau < \hbar/\epsilon_F\tau$, the expression for the magnetoconductance can not be given in closed form, and its derivation is more involved, since we must account for the orbit bending due to the magnetic field, the Lorentz force [65]. When the impurity mean free time τ becomes comparable to the phase coherence time τ_φ, we are no longer in the diffusive regime, and a Boltzmannian description must be introduced [66].

independent of sample parameters.[37] The magnetoresistance is therefore negative, $\Delta R = -\Delta G/G_{cl}^2$, which is a distinct sign that the effect is not classical, since we are considering a macroscopic system.[38]

The negative anomalous magnetoresistance can be understood qualitatively from the simple interference picture of the weak-localization effect. The presence of the magnetic field breaks the time-reversal invariance, and upsets the otherwise identical values of the phase factors in the amplitudes for traversing the time-reversed weak-localization loops. The quantum interference term for a loop c is due to the presence of the magnetic field changed according to

$$A_c\, A_{\tilde{c}}^* \;\to\; |A_c^{(B=0)}|^2 \exp\left\{\frac{2ie}{\hbar}\oint_c d\bar{\mathbf{x}}\cdot\mathbf{A}(\bar{\mathbf{x}})\right\} \;=\; |A_c^{(B=0)}|^2\, e^{\frac{2ie}{\hbar}\Phi_c}\,. \tag{11.178}$$

where Φ_c is the flux enclosed by the loop c. The weak-localization interference term acquires a random phase depending on the loop size, and the strength of the magnetic field, decreasing the probability of return, and thereby increasing the conductivity. The negative contribution from each loop in the impurity field to the conductance is modulated in accordance with the phase shift prescription for amplitudes by the oscillatory factor, giving the expression

$$< G(B) > - < G(O) > \;=\; \frac{e^2}{2\pi^2\hbar} < \sum_c |A_c^{(B=0)}|^2 \{1-\cos(2\pi\Phi_c/\Phi_0)\}\, e^{-t_c/\tau_\varphi} >_{imp} \tag{11.179}$$

The summation is over all classical loops in the impurity field returning to within a distance of the mean free path to a given point, and t_c is the duration for traversing the loop c, and Φ_0 is the flux quantum $\Phi_0 = 2\pi\hbar/2|e|$. The sum should be performed weighted with the probability for the realization of the loop in question, as expressed by the brackets. The weight of loops that are longer than the phase coherence length is suppressed, as their coherence are destroyed by inelastic scattering. In weak magnetic fields, only the longest loops are influenced by the phase shift due to the magnetic field. It is evident from eq.(11.179) that the low field magnetoconductance is positive and quadratic in the field.[39] The continuing monotonic behavior as a function of the magnetic field until saturation is simply a geometric property of diffusion, viz. that small diffusive loops are prolific. Instead of verifying this statement, let us turn the argument around and use our physical understanding of the weak localization effect to learn about the distribution of the areas of diffusive loops in two dimensions. Rewriting eq.(11.168) we have in two

[37] Experimental observations of the low field magnetoresistance of thin metallic films are in remarkable good agreement with the theory. The weak-localization effect is thus of importance for extracting information about inelastic scattering strengths, which is otherwise hard to come at. For reviews of the experimental results, see references [58] and [59].

[38] The classical magnetoresistance of a macroscopic sample calculated on the basis of the Boltzmann equation is positive.

[39] The minimum value of the magnetoresistance is *exactly* for zero magnetic field, and the weak localization effect is thus one of the few effects that can be used as a reference for zero magnetic field.

dimensions

$$C_0(\mathbf{x},\mathbf{x}) = \int_0^\infty dt\, e^{-t/\tau\varphi} \frac{B}{\tau\Phi_0} \sum_{n=0}^{n_{max}} e^{-\frac{4\pi BD_0}{\Phi_0}(n+1/2)t} . \tag{11.180}$$

For times $t > \tau$ we can let the summation run over all natural numbers and we can sum the geometric series to obtain

$$C_0(\mathbf{x},\mathbf{x}) = \int_0^\infty dt \frac{e^{-t/\tau\varphi}}{4\pi\tau D_0 t} \frac{2\pi BD_0 t}{\Phi_0} \frac{1}{\sinh\frac{2\pi BD_0 t}{\Phi_0}} \tag{11.181}$$

The factors independent of the magnetic field are the return probability and the dephasing factor. Representing the factors depending on the field strength, which describes the influence of the magnetic field on the quantum interference process, by its cosine transform

$$\frac{2\pi BD_0 t}{\Phi_0} \frac{1}{\sinh\frac{2\pi BD_0 t}{\Phi_0}} = \int_{-\infty}^\infty dS\, \cos\frac{SB}{\Phi_0} f_t(S) \tag{11.182}$$

and inverting gives

$$f_t(S) = \frac{1}{4D_0 t} \frac{1}{\cosh^2\left(\frac{S}{4D_0 t}\right)} . \tag{11.183}$$

We can therefore write for the weak localization contribution to the conductance

$$\delta G(B) = -\frac{2e^2 D_0 \tau}{\pi\hbar} \int_0^\infty dt \frac{e^{-t/\tau\varphi}}{4\pi\tau D_0 t} \int_0^\infty dS\, f_t(S) \cos\left(\frac{BS}{\Phi_0}\right) \tag{11.184}$$

and we note that $f_t(S)$ is normalized, and has the interpretation of the probability for a diffusive loop of duration t to enclose the area S.

For the average size of a diffusive loop of duration t we have

$$< S >_t \equiv \int_0^\infty dS\, S f_t(S) = 4D_0 t \ln 2 \tag{11.185}$$

i.e., the typical size of a diffusive loop of duration t is proportional to $D_0 t$.

For the fluctuations we have

$$< S^2 >_t \equiv \int_{-\infty}^\infty dS\, S^2 f_t(S) = 8\pi^2 (D_0 t)^2 \tag{11.186}$$

and we can write

$$f_t(S) = \frac{\pi}{\sqrt{2 < S^2 >_t}} \frac{1}{\cosh^2 \frac{\pi S}{\sqrt{2 < S^2 >_t}}} . \tag{11.187}$$

The probability distribution for diffusive loops is thus a steadily decreasing function of the area.

11.4.2 Three-Dimensional Sample

In the three-dimensional case we perform the Q_z-integration in eq.(11.165) and obtain

$$\delta\sigma(B) = -\frac{e^2}{\pi^3 l_B} \sum_{n=0}^{n_{max}} \frac{1}{\sqrt{n+\frac{1}{2}+\delta}} \tan^{-1}\left(\frac{l_B}{2l\sqrt{n+\frac{1}{2}+\delta}}\right) \tag{11.188}$$

where we have introduced

$$\delta = \frac{l_B^2}{4L_\varphi^2} = \frac{\hbar}{4D_0|e|B\tau_\varphi} . \tag{11.189}$$

In the low magnetic field limit, $\omega_c\tau \ll \hbar/\epsilon_F\tau$, the sum will approximately be given by the integral

$$\delta\sigma(B) = -\frac{e^2}{\pi^3\hbar l_B} \int_0^{n_{max}+1} dx \frac{1}{\sqrt{x+\delta}} \tan^{-1}\left(\frac{l_B}{2l\sqrt{x+\delta}}\right) \tag{11.190}$$

so that

$$\Delta\sigma(B) \equiv \delta\sigma(B) - \delta\sigma(B=0)$$

$$- \frac{e^2}{\pi^3\hbar l_B} \left(\int_0^{n_{max}+1} dx \frac{\tan^{-1}\frac{l_B}{2l\sqrt{x+\delta}}}{\sqrt{x+\delta}} - \sum_{n=0}^{n_{max}} \frac{\tan^{-1}(\frac{l_B}{2l\sqrt{n+\frac{1}{2}+\delta}}}{\sqrt{n+\frac{1}{2}+\delta}} \right) . \tag{11.191}$$

We should not forget about the upper cutoff. However, the subtraction renders the above expression well-defined. In the low magnetic field limit, $l_B \ll l$, where $n_{max} \gg 1$, we obtain the result

$$\Delta\sigma(B) = \frac{e^2}{\pi^3\hbar l_B} f_3(4|e|D_0 B\tau_\varphi) \tag{11.192}$$

where

$$f_3(x) = \sum_{n=0}^\infty \left\{ 2\left(\sqrt{n+1+\frac{1}{x}} - \sqrt{n+\frac{1}{x}}\right) - \frac{1}{\sqrt{n+\frac{1}{2}+\frac{1}{x}}} \right\} \tag{11.193}$$

To find the asymptotic limit of the function f_3 for small values, $x \ll 1$, we expand the above expression in $n + 1/2 + 1/x$ and obtain

$$f_3(x) = \frac{1}{32} \sum_{n=0}^\infty \left(n+1+\frac{1}{x}\right)^{-5/2} . \tag{11.194}$$

This Riemann zeta-function has the limits (see for instance reference [64] p. 1073)

$$f_3(x) = \begin{cases} \frac{1}{48} x^{3/2} & x \ll 1 \\ 0.605 & x \gg 1. \end{cases} \tag{11.195}$$

where in the limit of large x, the function f_3 is seen to approach a constant value which has been calculated numerically [67].

We note that the weak-localization magnetoresistance in three dimensions is independent of the relative directions of the magnetic field and the current; i.e., the longitudinal and transverse magnetoresistance are identical. Furthermore, we notice that at large magnetic fields the magnetoresistance tends to a universal constant (independent of sample parameters). The low-field square-root dependence of the magnetoconductance cleared up a long-standing mystery in the field of magnetotransport in doped semiconductors.

11.5 Aharonov-Bohm Effect

The most striking manifestation of the quantum interference involved in the weak-localization effect is obtained by confining the motion of the electrons to a thin cylindrical shell (or a ring), which is penetrated by a magnetic flux directed along the axis of the cylinder. In that case, all closed loops enclose the same flux $\Phi = B\pi R^2$, where R is the radius of the cylinder, and the conductivity should oscillate as a function of the flux Φ threading the cylinder with the period Φ/Φ_0. This is an example of the Aharonov-Bohm effect in solid state physics.[40]

We now turn to the quantitative description of the weak-localization Aharonov-Bohm effect, and must therefore solve the Cooperon equation in cylindrical coordinates

$$\left\{-D_0\left(\left(\frac{1}{R}\frac{\partial}{\partial\varphi}-\frac{2ie}{\hbar}A_\varphi\right)^2-\frac{\partial^2}{\partial z^2}\right)+\frac{1}{\tau_\varphi}\right\}C_0(z,z',\varphi,\varphi')=\frac{1}{\tau R}\,\delta(z-z')\,\delta(\varphi-\varphi')\,. \tag{11.196}$$

We have chosen a gauge where only the azimuthal component of the vector potential is nonzero, and we assume that the thickness a of the cylindrical shell satisfies the criterion $B^2L_\varphi^2\,a^2 \ll \Phi_0^2$. We can then assume that the vector potential is constant within the cylindrical shell, and we obtain the solution

$$C_0(z,z',\varphi,\varphi') \;=\; \frac{1}{2\pi RL_zD_0\tau}\sum_{n,Q_z}{}' \frac{e^{iQ_z(z-z')+in(\varphi-\varphi')}}{Q_z^2+(\frac{n}{R}-\frac{\Phi}{R\Phi_0})^2+L_\varphi^{-2}} \tag{11.197}$$

where the restriction to the singular regime requires $|n|, \Phi/\Phi_0 \ll R/l$. Assuming $l \ll R$, we can extend the n-summation to $\pm\infty$.

In the case of a ring, the quasi-one-dimensional case, $L_z \ll L_\varphi$, we only have to keep the $Q_z = 0$-term in the Q_z-sum. The summation over n is readily done by the method of residues

$$\sum_{n=-\infty}^{\infty}\frac{1}{(n-\frac{\Phi}{\Phi_0})^2+\left(\frac{R}{L_\varphi}\right)^2} \;=\; \sum_i res(g,z_i) \tag{11.198}$$

[40] This amazing manifestation of the quantum mechanical superposition principle at the macroscopic level was suggested in reference [68]. Here we follow the presentation of reference [69].

where

$$g(z) \;\equiv\; \pi\frac{\cos\pi z}{\sin\pi z}\,f(z) \quad , \quad f(z) \;\equiv\; \frac{1}{(z-\frac{\Phi}{R\Phi_0})^2+\left(\frac{R}{L_\varphi}\right)^2} \tag{11.199}$$

and we obtain for the flux dependence of the conductance of a ring

$$\delta G(\Phi) \;=\; -\frac{e^2}{\pi\hbar}\,L_\varphi\,\frac{\sinh\frac{2\pi R}{L_\varphi}}{\cosh\frac{2\pi R}{L_\varphi}-\cos\frac{2\pi\Phi}{\Phi_0}}\,. \tag{11.200}$$

In the limit $R \ll L_\varphi$ (which can be achieved for an arbitrary large radius by lowering the temperature) we get the result

$$\delta G(\Phi) \;=\; -\frac{2e^2}{\hbar}\,R\,\frac{1}{1+\frac{1}{2}\left(\frac{2\pi R}{L_\varphi}\right)^2-\cos\frac{2\pi\Phi}{\Phi_0}}\,. \tag{11.201}$$

We note that the modulation amplitude can be made arbitrarily large.

In the case of a cylinder, the quasi-two-dimensional case, we have for the flux dependence of the conductance

$$\delta G(\Phi) \;=\; -\frac{2e^2}{\pi\hbar}\,\frac{1}{2\pi R}\int_{-1/l}^{1/l}dQ_z\sum_{n=-\infty}^{\infty}\frac{1}{Q_z^2+\frac{1}{R^2}(n-\frac{\Phi}{\Phi_0})^2+L_\varphi^{-2}}\,. \tag{11.202}$$

We improve the convergence by adding and subtracting the zero-flux result, and can then extend the Q_z-integration to $\pm\infty$, and obtain (see for example the table of integrals [64] p. 978)

$$\begin{aligned}\Delta G(\Phi) \;&\equiv\; \delta G(\Phi)-\delta G(\Phi=0)\\ &=\; -\frac{e^2}{\pi^2\hbar}\left\{\ln\frac{L_\varphi}{l}\;-\;2\sum_{n=1}^{\infty}K_0\left(\frac{2\pi Rn}{L_\varphi}\right)\left(1-\cos\frac{2\pi n\Phi}{\Phi_0}\right)\right\}\end{aligned} \tag{11.203}$$

where K_0 is the modified Bessel function, the McDonald function. The flux dependence tends to zero exponentially for $R \gg L_\varphi$, and in the opposite limit, $R \ll L_\varphi$ (achieved at low temperatures) the amplitude of the flux modulation will tend to infinity since

$$K_0(x) \;=\; \begin{cases}\sqrt{\frac{\pi}{2x}}\,e^{-x} & \text{for } x \gg 1\\ -\ln x & \text{for } x \ll 1\,.\end{cases} \tag{11.204}$$

For a review of the experimental confirmation of the weak-localization Aharonov-Bohm effect, we refer to reference [70].

11.6 Magnetic-Impurity and Spin-Orbit Scattering

In this section we take into account spin-orbit scattering off the impurities and allow for the impurities to accommodate magnetic scattering.[41] On general physical grounds we deduce that magnetic-impurity scattering destroys quantum interference since the electronic path is partially kept track of, due to the flipped impurity spins revealing the visit of an electron, and quantum interference between distinguishable trajectories is excluded. Spin-orbit scattering, in contrast to magnetic-impurity scattering, does not violate time-reversal symmetry, and one could be inclined to assert that it should have no influence on the weak-localization quantum interference. However, the coupling between the orbital and spin degrees of freedom of an electron provided by the spin-orbit scattering leads to highly nontrivial effects.

To accommodate the additional scattering mechanisms, the impurity potential matrix element has to be changed from merely a constant (in the momentum representation) to the scattering amplitude

$$f_{\alpha\alpha'}(\mathbf{p},\mathbf{p}') \;=\; V\,\delta_{\alpha\alpha'} \;+\; V_S\,\mathbf{S}_i\cdot\vec{\sigma}_{\alpha\alpha'} \;-\; i\,V_{so}\,(\mathbf{p}\times\mathbf{p}')\cdot\vec{\sigma}_{\alpha\alpha'} \tag{11.205}$$

where $\mathbf{S}_i$ and $\vec{\sigma}$ denote the impurity and electron spin, respectively. Performing the standard positional impurity averaging, we obtain in the Born approximation the impurity correlator

$$\begin{aligned} U_{\alpha\alpha';\beta\beta'}(\mathbf{p},\mathbf{p}') \;&=\; n_i\Big(|V|^2\,\delta_{\alpha\alpha'}\,\delta_{\beta\beta'} \;+\; |V_s|^2\,\mathbf{S}_i^2\,\vec{\sigma}_{\alpha\alpha'}\cdot\vec{\sigma}_{\beta\beta'} \\ &-\; |V_{so}|^2\,(\mathbf{p}\times\mathbf{p}')\cdot\vec{\sigma}_{\alpha\alpha'}\,(\mathbf{p}'\times\mathbf{p})\cdot\vec{\sigma}_{\beta\beta'}\Big) \end{aligned}$$

$$\equiv$$

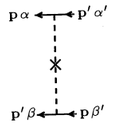

. (11.206)

Diagrammatically we have the Cooperon equation

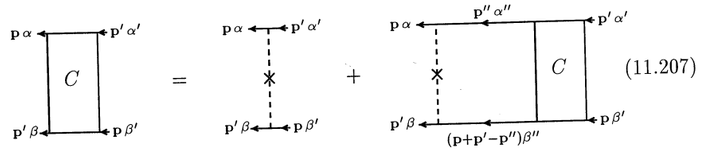

(11.207)

[41] We follow the presentation in reference [71]. Magnetoresistance in many-valley semiconductors is discussed in reference [72].

Due to the orbital structure of the spin-orbit scattering the Cooperon equation will in general be a complicated integral equation in the angular variables. However, in the limit, $\tau_{so},\tau_s \gg \tau$, where an electron changes momentum many times before its spin is flipped the integral kernel, the correlator eq.(11.206), can be approximated by its average over momentum directions, the Fermi surface average. We thus get the following equation for the Cooperon:

$$C_{\alpha\alpha';\beta\beta'}(\mathbf{p},\mathbf{p}') \;=\; \overline{U}_{\alpha\alpha';\beta\beta'} + \overline{U}_{\alpha\alpha'';\beta\beta''}\,\tilde{\zeta}(\mathbf{Q},\omega)\,C_{\alpha''\alpha';\beta''\beta'}(\mathbf{Q},\omega) \tag{11.208}$$

where the Fermi surface averaged impurity correlator has the form:

$$\overline{U}_{\alpha\alpha';\beta\beta'} \;=\; u^2\,\delta_{\alpha\alpha'}\,\delta_{\beta\beta'} \;+\; \frac{1}{3}(u_s^2-u_{so}^2)\vec{\sigma}_{\alpha\alpha'}\cdot\vec{\sigma}_{\beta\beta'} \tag{11.209}$$

with

$$u_s^2 \;=\; n_i|V_s|^2 < \mathbf{S}_i^2 > \tag{11.210}$$

and

$$u_{so}^2 \;=\; n_i|V_{so}|^2\,\overline{(\mathbf{p}\times\mathbf{p}')}\,. \tag{11.211}$$

The bracket denotes an average over the assumed random directions of the impurity spins, and the bar denotes the Fermi surface average. The insertion is, $\hbar\mathbf{Q}\equiv\mathbf{p}+\mathbf{p}'$,

$$\tilde{\zeta}(\mathbf{Q},\omega) \;=\; 2\pi N_0\tau'\left(1+i\omega\tau'-D_0\tau'\mathbf{Q}^2\right) \tag{11.212}$$

where τ' is the total elastic scattering time

$$\frac{1}{\tau'}=\frac{1}{\tau}+\frac{1}{\tau_s}+\frac{1}{\tau_{so}}\;,\;\; \frac{\hbar}{\tau_s}=2\pi N_0 u_s^2\;,\;\; \frac{\hbar}{\tau_{so}}=2\pi N_0 u_{so}^2\,. \tag{11.213}$$

The form of the insertion $\tilde{\zeta}$ is a simple consequence of the averaged propagator for the present case being diagonal in the spin degrees of freedom and given by

$$G^{R(A)}_{\alpha\beta}(E,\mathbf{p}) \;=\; \frac{1}{E-\epsilon_{\mathbf{p}}\,(^{+}_{-})\,\frac{i\hbar}{2\tau'}}\;\delta_{\alpha\beta}\,. \tag{11.214}$$

We have assumed three-dimensionality with respect to spin-scattering properties so that[42]

$$\frac{1}{\tau_s^x}=\frac{1}{\tau_s^y}=\frac{1}{\tau_s^z}=\frac{1}{3}\,\frac{1}{\tau_s} \tag{11.215}$$

and

$$\frac{1}{\tau_{so}^x}=\frac{1}{\tau_{so}^y}=\frac{1}{\tau_{so}^z}=\frac{1}{3}\,\frac{1}{\tau_{so}} \tag{11.216}$$

where

$$\frac{\hbar}{\tau_s}=2\pi N_0 u_s^2 \tag{11.217}$$

[42] In a system where the motion of the electrons are strictly two-dimensional, the spin-orbit scattering is seen to be absent for the considered scattering mechanism, since a coupling $\hat{z}\cdot\vec{\sigma}$ can not flip the spin along the z-direction.

and

$$\frac{\hbar}{\tau_{so}} = 2\pi N_0 u_{so}^2 \,. \tag{11.218}$$

The spin structure of the Cooperon, determined by the spin structure of the impurity correlator, is given by

$$C_{\alpha\alpha';\beta\beta'} \;=\; A(\mathbf{Q},\omega)\,\delta_{\alpha\alpha'}\,\delta_{\beta\beta'} \;+\; B(\mathbf{Q},\omega)\,\vec{\sigma}_{\alpha\alpha'}\cdot\vec{\sigma}_{\beta\beta'}\,. \tag{11.219}$$

Using the identity

$$(\vec{\sigma}_{\alpha\alpha''}\cdot\vec{\sigma}_{\beta\beta''})(\vec{\sigma}_{\alpha''\alpha'}\cdot\vec{\sigma}_{\beta''\beta'}) \;=\; 3\,\delta_{\alpha\alpha'}\,\delta_{\beta\beta'} \;-\; 2\,\vec{\sigma}_{\alpha\alpha'}\cdot\vec{\sigma}_{\beta\beta'} \tag{11.220}$$

it is straightforward, in the limit $\tau \ll \tau_{so}, \tau_s$, to obtain

$$A(\mathbf{Q},\omega) \;=\; \frac{1}{2\tau}\left(\frac{\frac{3}{2}}{-i\omega + D_0\mathbf{Q}^2 + \frac{2}{3\tau_s} + \frac{4}{3\tau_{so}}} \;+\; \frac{\frac{1}{2}}{-i\omega + D_0\mathbf{Q}^2 + \frac{2}{\tau_s}}\right) \tag{11.221}$$

and

$$B(\mathbf{Q},\omega) \;=\; \frac{1}{\frac{2}{3}\tau}\left(\frac{1}{-i\omega + D_0\mathbf{Q}^2 + \frac{2}{3\tau_s} + \frac{4}{3\tau_{so}}} \;-\; \frac{1}{-i\omega + D_0\mathbf{Q}^2 + \frac{2}{\tau_s}}\right). \tag{11.222}$$

We thus have the following conductivity correction

$$\delta\sigma(\omega) \;=\; -\frac{e^2 D_0}{\pi\hbar L^d}\sum_{\mathbf{Q}}{}' C_{\alpha\beta;\beta\alpha}(\mathbf{Q},\omega) \;=\; -\frac{e^2 D_0}{\pi\hbar L^d}\sum_{\mathbf{Q}}{}' 2\Big(A(\mathbf{Q},\omega) + 3\,B(\mathbf{Q},\omega)\Big)$$

$$= -\frac{2e^2 D_0}{\pi\hbar L^d}\sum_{\mathbf{Q}}{}'\left(\frac{\frac{3}{2}}{-i\omega + D_0\mathbf{Q}^2 + \frac{2}{3\tau_s} + \frac{4}{3\tau_{so}}} \;-\; \frac{\frac{1}{2}}{-i\omega + D_0\mathbf{Q}^2 + \frac{2}{\tau_s}}\right). \tag{11.223}$$

We notice that the magnetic impurity scattering in accordance with our expectation suppresses the weak-localization effect. In the absence of magnetic scattering, we observe that the spin-orbit scattering will not eliminate the singularity in the conductivity, but instead change the sign of the quantum correction (and reduce the strength by a factor of 2)! This effect is referred to as weak antilocalization, and has been observed in many substances for which impurities give rise to strong spin-orbit scattering. The scaling function will thus for the case of spin-orbit scattering cross the axis as in the three-dimensional case, before it at large conductance approaches zero, i.e., exhibit nonmonotonic behavior.[43] We have assumed that the sample length L is much greater than the spin-orbit length scale, $L_{so} \equiv \sqrt{D_0\tau_{so}}$, the length scale for randomizing the spin direction due to spin-orbit scattering. The scaling function thus depends on the symmetry of the scattering potential.

[43]Such a nontrivial scaling behavior seems to be confirmed by a four-loop renormalization group calculation [73]. Due to the importance of high-order terms in the perturbative expansion of the scaling function (here the importance of the finite $1/g^5$-term) a self-consistent theory of localization for systems with spin-orbit scattering has not been achieved.

If we decompose the spin states in singlet,

$$C_s(\mathbf{Q},\omega) \;=\; A(\mathbf{Q},\omega) \;-\; 3B(\mathbf{Q},\omega) \;=\; \frac{1}{-i\omega + D_0\mathbf{Q}^2 + \frac{2}{\tau_s}} \tag{11.224}$$

and triplet,

$$C_t(\mathbf{Q},\omega) \;=\; A(\mathbf{Q},\omega) \;+\; B(\mathbf{Q},\omega) \;=\; \frac{1}{-i\omega + D_0\mathbf{Q}^2 + \frac{2}{3\tau_s} + \frac{4}{3\tau_{so}}} \tag{11.225}$$

we recognize that the singlet part of the Cooperon is unaffected by spin-orbit scattering.

The weak antilocalization effect; i.e., the appearance of the minus sign is a consequence of the interference being between time-reversed scattering sequences. On the time-reversed trajectory the electron experiences the spin rotations in opposite sequence and opposite directions

$$\psi_c \;=\; \underline{\underline{R}}\,\psi_i\,, \qquad \psi_{\bar{c}} \;=\; \underline{\underline{R}}^{-1}\,\psi_i \tag{11.226}$$

where

$$\underline{\underline{R}}(\phi,\theta,\psi) \;=\; \begin{pmatrix} e^{\frac{i}{2}(\phi+\psi)}\cos\frac{\theta}{2} & i\sin\frac{\theta}{2}e^{\frac{i}{2}(\psi-\phi)} \\ i\sin\frac{\theta}{2}e^{-\frac{i}{2}(\psi-\phi)} & e^{-\frac{i}{2}(\phi+\psi)}\cos\frac{\theta}{2} \end{pmatrix} \tag{11.227}$$

is the unitary rotation operator in spin space parametrized by the Euler angles (recall exercise 1.10 on page 50). For the following example of initial spin state represented by the spinor

$$\psi_i \;=\; \begin{pmatrix} 1 \\ 0 \end{pmatrix} \tag{11.228}$$

we have for the final spin states for the two interfering alternatives

$$\psi_c \;=\; \begin{pmatrix} R_{11} \\ R_{12} \end{pmatrix}, \qquad \psi_{\bar{c}} = \begin{pmatrix} R_{11}^* \\ R_{21}^* \end{pmatrix} \;=\; \begin{pmatrix} R_{11}^* \\ -R_{12} \end{pmatrix} \tag{11.229}$$

where we notice the appearance of a minus sign. For the interference term we then get

$$\psi_c^*\psi_{\bar{c}} + \psi_{\bar{c}}^*\psi_c \;=\; R_{11}^*R_{11}^* + R_{12}^*R_{21}^* + R_{11}R_{11} + R_{21}R_{12} \;=\; 2\,\Re e(R_{11}^2 - |R_{12}|^2)$$

$$=\; 2\,\Re e\left(\cos^2\frac{\theta}{2}\,e^{i(\phi+\psi)} - \sin^2\frac{\theta}{2}\right) \tag{11.230}$$

The first term in the parentheses averages to zero due to the random phase factor, whereas the second term on the average produces the factor $-1/2$ in eq.(11.223).

The magnetoresistance calculation in the presence of spin-flip and spin-orbit scattering is parallel to the one already performed in section 11.4, and without repeating it we notice that it corresponds to the substitution $D_0Q^2 \to 4D_0|e|B\tau\hbar^{-1}$, and we obtain for the magnetoconductivity in the two-dimensional case

$$\Delta\sigma(B) \;=\; -\frac{e^2}{2\pi^2\hbar}\left(\psi\left(\frac{1}{2}+\frac{B_1}{B}\right) \;-\; \frac{3}{2}\,\psi\left(\frac{1}{2}+\frac{B_2}{B}\right) \;+\; \frac{1}{2}\,\psi\left(\frac{1}{2}+\frac{B_3}{B}\right)\right) \tag{11.231}$$

where

$$B_1 = B_\tau + B_{so} + B_s \ , \ B_2 = \frac{4}{3}B_{so} + \frac{2}{3}B_s + B_\varphi \ , \ B_3 = 2B_s + B_\varphi \qquad (11.232)$$

and we have introduced the characteristic elastic magnetic field scales

$$B_\tau = \frac{\hbar}{4D_0|e|\tau} \ , \ B_{so} = \frac{\hbar}{4D_0|e|\tau_{so}} \ , \ B_s = \frac{\hbar}{4D_0|e|\tau_s} \ . \qquad (11.233)$$

A sample with spin-orbit scattering will thus show a positive magnetoresistance, and the extremal value at zero magnetic field will be a minimum.[44]

11.7 Mesoscopic Fluctuations

In the following we shall show that when the size of a sample becomes comparable to the phase coherence length, $L \sim L_\varphi$, the individuality of the sample will be manifest in its transport properties. Such a sample is said to be mesoscopic. Characteristically the conductance will exhibit sample-specific, noiselike but reproduceable, aperiodic oscillations as a function of, say, magnetic field or chemical potential (i.e., density of electrons). The sample behavior is thus no longer characterized by its average characteristics, such as the average conductance, i.e., the average impurity concentration. The statistical assumption of phase-incoherent and therefore independent subsystems, allowing for such an average description, is no longer valid when the transport takes place quantum mechanically coherently throughout the whole sample. As a consequence, a mesoscopic sample does not possess the property of being self-averaging; i.e., the relative fluctuations in the conductance do not vanish in a central limit fashion inversely proportional to the volume in the large-volume limit. To describe the fluctuations from the average value we need to study the higher moments of the conductance distribution such as the variance $\Delta G_{\alpha\beta,\gamma\delta}$. We shall first study the fluctuations in the conductance at zero temperature, and consider the variance

$$\Delta G_{\alpha\beta,\gamma\delta} \ = \ < (G_{\alpha\beta} - < G_{\alpha\beta} >)(G_{\gamma\delta} - < G_{\gamma\delta} >) > \ . \qquad (11.234)$$

For the conductance fluctuations we have the expression

$$< G_{\alpha\beta}\, G_{\gamma\delta} > \ = \ (L^{-2})^2 \int d\mathbf{x}_2 \int d\mathbf{x}'_2 \int d\mathbf{x}_1 \int d\mathbf{x}'_1 \, < \sigma_{\alpha\beta}(\mathbf{x}_2, \mathbf{x}'_2)\, \sigma_{\gamma\delta}(\mathbf{x}_1, \mathbf{x}'_1) > \ . \qquad (11.235)$$

The diagrams for the variance of the conductance fluctuations can still be managed within the standard impurity diagram technique in the weak disorder limit, $\epsilon_F \tau \gg \hbar$, and a typical conductance fluctuation diagram is depicted in figure 11.4. (here the box denotes the Diffuson).[45]

[44] An elegant verification of the weak antilocalization effect was demonstrated in experiments by Bergmann [58], where a thin film of magnesium where spin-orbit scattering is absent, were covered with an increasing amount of a submonolayer of gold, thereby increasing the spin-orbit scattering.

[45] The diagram is in the position representation, and the momentum labels should presently be ignored, but will be explained shortly.

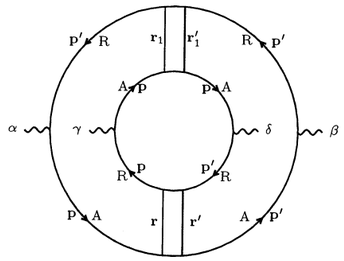

Figure 11.4 Conductance fluctuation diagram.

The construction of the conductance fluctuation diagrams follows from impurity averaging two conductivity diagrams: Draw two conductivity bubble diagrams, where the propagators include the impurity scattering. Treating the impurity scattering perturbatively, we get impurity vertices that we, upon averaging them, have to pair in all possible ways. Since we subtract the squared average conductance in forming the variance, ΔG, the diagrams for the variance consist only of diagrams where the two conductance loops are connected by impurity lines. As already noted in the discussion of weak localization, the dominant contributions to such loop-type diagrams are from the infrared and long-wavelength divergence of the Cooperon, and here additionally from the Diffuson.

To calculate the contribution to the variance from the Diffuson diagram depicted in figure 11.4, we write the corresponding expression down in the spatial representation in accordance with the usual Feynman rules for conductivity diagrams. Let us consider a hypercube of size L. If we assume that the sample size is bigger than the impurity mean free path, $L > l$, the spatial extension of the integration over the external, excitation and measuring, vertices can be extended to infinity, since the propagators has the spatial extension of the mean free path. We can therefore introduce the Fourier transform for the propagators since no reference to the finiteness of the system is necessary for such local quantities. Furthermore, since the spatial extension of the Diffuson is long range compared to the mean free path, we can set the spatial labels of the Diffusons equal to each other, i.e., $\mathbf{r}_1 = \mathbf{r}$ and $\mathbf{r}'_1 = \mathbf{r}'$. All the spatial integrations, except the ones determined by the Diffuson, can then be performed, leading to the momentum labels for the propagators as depicted in figure 11.4. Let us study the fluctuations in the dc conductance, so that the frequency, ω, of the external field is zero. The energy labels have for visual clarity been deleted from figure 11.4, since we only have elastic scattering and therefore one label, say ϵ, for the outer ring and one for the inner, ϵ'. According to the Feynman rules, we obtain for the Diffuson diagram

the following analytical expression:

$$< G_{\alpha\beta}G_{\gamma\delta} >_D = L^{-4}\left(\frac{e^2\hbar^2u^2}{4\pi m^2}\right)^2 \int_{-\infty}^{\infty}d\epsilon \frac{\partial f(\epsilon)}{\partial\epsilon}\int_{-\infty}^{\infty}d\epsilon' \frac{\partial f(\epsilon')}{\partial\epsilon'}\int\frac{d\mathbf{p}}{(2\pi\hbar)^3}\int\frac{d\mathbf{p}'}{(2\pi\hbar)^3}$$

$$G^R_\epsilon(\mathbf{p}')G^A_\epsilon(\mathbf{p}')G^A_{\epsilon'}(\mathbf{p}')G^R_{\epsilon'}(\mathbf{p}')G^R_\epsilon(\mathbf{p})G^A_{\epsilon'}(\mathbf{p})G^A_\epsilon(\mathbf{p})G^R_{\epsilon'}(\mathbf{p})$$

$$p_\alpha\, p_\gamma\, p'_\delta\, p'_\beta \int d\mathbf{r}\int d\mathbf{r}'\, |D(\mathbf{r},\mathbf{r}',\epsilon-\epsilon')|^2\ . \tag{11.236}$$

In order to obtain the above expression we have noted that

$$D(\mathbf{r},\mathbf{r}',\epsilon'-\epsilon) = [D(\mathbf{r},\mathbf{r}',\epsilon-\epsilon')]^* \tag{11.237}$$

which follows from the relationship between the retarded and advanced propagators. At zero temperature, the Fermi functions set the energy variables in the propagators in the conductance loops to the Fermi energy, and the Diffuson frequency to zero. At zero temperature we therefore get for the considered Diffuson diagram the following analytical expression, $D(\mathbf{r},\mathbf{r}') \equiv D(\mathbf{r},\mathbf{r}',0)$,

$$< G_{\alpha,\beta}G_{\gamma,\delta} >_D = L^{-4}\left(\frac{e^2\hbar^2u^2}{4\pi m^2}\right)^2 \int\frac{d\mathbf{p}}{(2\pi\hbar)^3}\int\frac{d\mathbf{p}'}{(2\pi\hbar)^3}\, p_\alpha\, p_\gamma\, p'_\delta\, p'_\beta$$

$$[G^R_{\epsilon_F}(\mathbf{p})G^A_{\epsilon_F}(\mathbf{p})G^R_{\epsilon_F}(\mathbf{p}')G^A_{\epsilon_F}(\mathbf{p}')]^2 \int d\mathbf{r}\int d\mathbf{r}'\, |D(\mathbf{r},\mathbf{r}')|^2\ . \tag{11.238}$$

It is important to note that the same Diffuson appears twice. This is the leading singularity we need to keep track of. If we try to construct variance diagrams containing, say, three Diffusons, we will observe that they cannot carry the same wave vector, and will give a contribution smaller by the factor $\hbar/\epsilon_F\tau$. The momentum integrations at the current vertices can easily be performed by the residue method

$$j_{\alpha\gamma} = \int\frac{d\mathbf{p}}{(2\pi\hbar)^3}\, p_\alpha\, p_\gamma\, [G^R_{\epsilon_F}(\mathbf{p})G^A_{\epsilon_F}(\mathbf{p})]^2 = \frac{4\pi}{3}\hbar p_F^2 N_0\,\tau^3\,\delta_{\alpha\gamma} \tag{11.239}$$

and we obtain for the considered Diffuson diagram the expression

$$< G_{\alpha\beta}G_{\gamma\delta} >_D = L^{-4}\left(\frac{e^2D_0\tau}{2\pi\hbar}\right)^2 \delta_{\alpha\gamma}\,\delta_{\delta\beta}\int d\mathbf{r}\int d\mathbf{r}'\, |D(\mathbf{r},\mathbf{r}')|^2\ . \tag{11.240}$$

To calculate the Diffuson integrals we need to address the finite size of the sample and its attachment to the current leads, since the Diffuson has no inherent length scale cutoff. At the surface where the sample is attached to the leads, the Diffuson vanishes

$$D(\mathbf{r},\mathbf{r}') = 0 \qquad \mathbf{r} \ \ or \ \ \mathbf{r}' \ \ \text{on lead surfaces} \tag{11.241}$$

in accordance with the assumption, that once an electron reaches the lead it never returns to the disordered region phase coherently. On the other surfaces the current

vanishes; i.e., the normal derivative of the Diffuson must vanish (recall eq.(5.200) and eq.(5.201))

$$\frac{\partial D(\mathbf{r},\mathbf{r}')}{\partial\mathbf{n}} = 0 \qquad \mathbf{r} \ \ or \ \ \mathbf{r}' \ \ \text{on lead surfaces with surface normal} \ \ \mathbf{n}\ . \tag{11.242}$$

We assume that the leads have the same size as the sample surface.[46] Therefore by solving the diffusion equation for the Diffuson, with the above mixed (von Neumann and Dirichlet) boundary condition, we obtain the expression

$$\int d\mathbf{r}\int d\mathbf{r}'\, |D(\mathbf{r},\mathbf{r}')|^2 = \left(\sum_n \frac{1/\tau}{D_0\, q_n^2}\right)^2 \tag{11.243}$$

where $n \equiv (n_x, n_y, n_z)$ is the eigenvalue index in the three-dimensional case

$$q_{n_\alpha} = \frac{\pi}{L}n_\alpha \qquad n_\alpha = n_x, n_y, n_z \tag{11.244}$$

where

$$n_x = 1, 2, ..., \qquad n_{y,z} = 0, 1, 2, ... \tag{11.245}$$

and we have assumed that the current leads are along the x-axis. Less than three dimensions corresponds to neglecting the n_y and n_z's. We therefore obtain from the considered Diffuson diagram the contribution to the conductance fluctuations[47]

$$< G_{\alpha\beta}G_{\gamma\delta} >_D = \left(\frac{e^2}{4\pi\hbar}\right)^2 c_d\ \delta_{\alpha,\gamma}\,\delta_{\delta,\beta} \tag{11.246}$$

where the constant c_d depends on the sample dimension. The summation in eq.(11.243) should, in accordance with the validity of the diffusion regime, be restricted to values satisfying $n_x^2+n_y^2+n_z^2 \le N$, where N is of the order of $(L/l)^2$. However, the sum converges rapidly and the constants c_d are seen to be of order unity. The dimensionality criterion is essentially the same as in the theory of weak localization, as we shall show in the discussion below of the physical origin of the fluctuation effects. The important thing to notice is that the long-range nature of the Diffuson provides the L^4 factor that makes the variance, average of the squared conductance, independent of sample size (recall eq.(7.142)). The diagram depicted in figure 11.4 is only one of the two possible pairings of the current vertices, and we obtain an additional contribution from the diagram where, say, current vertices γ and δ are interchanged.

In addition to the contribution from the diagram in figure 11.4 there is the other possible singular Diffuson contribution to the variance from the diagram depicted in figure 11.5.

[46] This "thick lead" assumption is not of importance. Because of the relationship between the fluctuations in the density of states and the time scale for diffusing out of the sample, the result will be the same for any kind of lead attachment [74].

[47] Because of these inherent mesoscopic fluctuations, we realize that the conductance discussed in the scaling theory of localization is the average conductance.

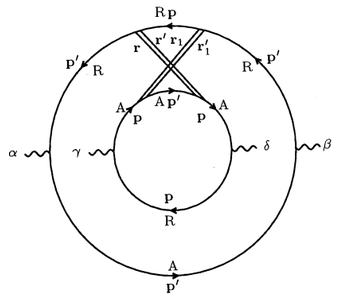

Figure 11.5 The other possible conductance fluctuation diagram.

This diagram contributes the same amount as the one in figure 11.4, but with a different pairing of the current vertices. We note that the diagram in figure 11.5 allows for only one assignment of current vertices.[48]

Reversing the direction in one of the loops gives rise to similar diagrams, but now with the Cooperon appearing instead of the Diffuson. Because the boundary conditions on the Cooperon are the same as for the Diffuson, in the absence of a magnetic field, the Cooperon contributes an equal amount. For the total contribution to the variance of the conductance, we therefore have (allowing for the spin degree of freedom of the electron would quadruple the value) at zero temperature

$$< G_{\alpha\beta} G_{\gamma\delta} > = \left(\frac{e^2}{2\pi\hbar}\right)^2 c_d \left(\delta_{\alpha\gamma}\,\delta_{\delta\beta} + \delta_{\alpha\delta}\,\delta_{\gamma\beta} + \delta_{\alpha,\beta}\,\delta_{\gamma,\delta}\right) \qquad (11.247)$$

The variance of the conductance at zero temperature, and for the chosen geometry of a hypercube, is seen to be independent of size and dimension of the sample and degree of disorder, and the conductance fluctuations appear in the metallic regime described above to be universal.[49]

Since the average classical conductance, according to eq.(8.74), is proportional to L^{d-2}, Ohm's law, we find that the relative variance, $\Delta G < G >^{-2}$, is proportional to L^{4-2d}. This result should be contrasted with the behavior L^{-2d} of thermodynamic fluctuations, compared to which the quantum interference induced mesoscopic fluctuations are huge, reflecting the absence of self-averaging.

The dominating role of the lowest eigenvalue in eq.(11.243) indicates that mesoscopic fluctuations, studied in situations with less invasive probes than the current leads necessary for studying conductance fluctuations, can be enhanced compared

[48]The contribution from the diagram in figure 11.4 can, through the Einstein relation, be ascribed to fluctuations in the diffusion constant, whereas the diagram in figure 11.5 gives the contribution from the fluctuations in the density of states, the two types of fluctuations being independent [75].

[49]However, for a noncubic sample, the variance will be geometry dependent, [76], [77].

to the universal value. In the case of the conductance fluctuations, the necessary connection of the disordered region to the leads, which cut off the singularity in the Diffuson by the lowest eigenvalue, $n_x = 1$, reflecting the fact that due to the physical boundary conditions at the interface between sample and leads, the maximal time for quantum interference processes to occur uninterrupted is the time it takes the electron to diffuse across the sample, L^2/D_0. When considering other ways of observing mesoscopic fluctuations, the way of observation will in turn introduce the destruction of phase coherence necessary for rendering the fluctuations finite.

In order to understand the origin of the conductance fluctuations, we note that, just as the conductance essentially is given by the probability for diffusing between points in a sample, the variance is likewise the product of two such probabilities. When we perform the impurity average, certain of the quantum interference terms will not be averaged away, since certain pairs of paths are coherent. This is similar to the case of coherence involved in the weak-localization effect, but in the present case of the variance of quite a different nature. For example, the quantum interference process described by the diagram in figure 11.4 is depicted in figure 11.6, where the solid line corresponds to the outer conductance loop, and the dashed line to the inner conductance loop. The wavy portion of the lines corresponds to the long-range diffusion process.

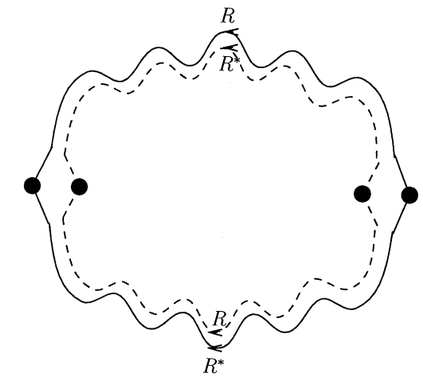

Figure 11.6 Statistical correlation described by the diagram in figure 11.4.

When one takes the impurity average of the variance, the quantum interference terms can pair up for each diffusive path in the random potential, but now they correspond to amplitudes for propagation in different samples. The diagrams for the variance, therefore, do not describe any physical quantum interference process, since we are not describing a probability but a product of probabilities. The variance gives the statistical correlation between amplitudes in different samples. The interference process corresponding to the diagram in figure 11.5 is likewise

depicted in figure 11.7.

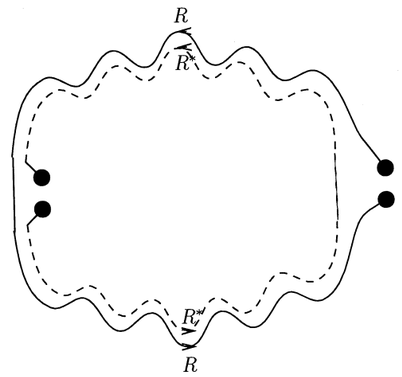

Figure 11.7 Statistical correlation described by the diagram in figure 11.5.

When a specific mesoscopic sample is considered, no impurity average is effectively performed as in the macroscopic case. The quantum interference terms in the conductance, which for a macroscopic sample averages to zero if we neglect the weak-localization effect, are therefore responsible for the mesoscopic fluctuations. In the weak-disorder regime the conductivity (or equivalently the diffusivity by Einstein's relation) is specified by the probability for the particle to propagate between points in space. According to eq.(11.17)

$$P = P_{cl} + 2 \sum_{c,c'} \sqrt{|A_c A_{c'}'|} \cos(\phi_c - \phi_{c'}) \tag{11.248}$$

as

$$A_c = |A_c| e^{i\phi_c} \quad , \quad \phi_c = \frac{1}{\hbar} S[\mathbf{x}_c(t)] \tag{11.249}$$

where $|A_c|$ specifies the probability for the classical path c, and its phase is specified by the action. When the points in space in questions are farther apart than the mean free path, the ensemble average of the quantum interference term in the probability vanishes. The weak localization can be neglected because for random phases we have $< \cos(\phi_c - \phi_{c'}) >_{imp} = 0$. However, for the mean square of the probability, we encounter $<\cos^2(\phi_c - \phi_{c'}) >_{imp} = 1/2$, and obtain

$$< P^2 >_{imp} = < P >^2_{imp} + 2 \sum_{c,c'} |A_c| |A_c'| \, . \tag{11.250}$$

Because of quantum interference there is thus a difference between $< P^2 >_{imp}$ and $< P >^2_{imp}$ resulting in mesoscopic fluctuations. Since the effect is determined by the phases of paths, it is nonlocal.

The result in eq.(11.247) is valid in the metallic regime, where the average conductance is larger than $e^2/2\pi\hbar$. To go beyond the metallic regime would necessitate introducing the quantum corrections to diffusion, the first of which is the weak-localization type, which diagrammatically corresponds to inserting Cooperons in between Diffusons. Such an analysis is necessary for a study of the fluctuations in the strongly disordered regime, as performed in reference [44].

The Diffuson and Cooperon in the conductance fluctuation diagrams do not describe diffusion and return probability, respectively, in a given sample, but quantum-statistical correlations between motion in different samples, i.e., different impurity configurations, as each conductance loop in the figures 11.4 and 11.5 corresponds to different samples. In order to stress this important distinction, we shall in the following mark with a tilde the Diffusons and Cooperons appearing in fluctuation diagrams.

We now assess the effects of finite temperature on the conductance fluctuations. Besides the explicit temperature dependence due to the Fermi functions appearing in eq.(11.236), the ladder diagrams will be modified by interaction effects. The presence of the Fermi functions corresponds to an energy average over the thermal layer near the Fermi surface, and through the energy dependence of the Diffuson and Cooperon introduces the temperature-dependent length scale $L_T = \sqrt{D_0 \hbar / kT}$. Since the loops in the fluctuation diagrams correspond to different conductivity measurements, i.e., different samples, interaction lines (due to for example electron-phonon or electron-electron interaction) are not allowed to connect the loops in a fluctuation diagram. The diffusion pole of the Diffuson appearing in a fluctuation diagram is therefore not immune to interaction effects. This was only the case when the Diffuson describes diffusion within a sample, since then the diffusion pole is a consequence of particle conservation and therefore unaffected by interaction effects. The consequence is that, just as in the case for the Cooperon, inelastic scattering will lead to a cutoff given by the phase-breaking rate $1/\tau_\varphi$. In short, the temperature effects will therefore ensure that up to the length scale of the order of the phase-coherence length, the conductance fluctuations are determined by the zero-temperature expression, and beyond this scale the conductance of such phase-incoherent volumes add as in the classical case.[50] A sample is therefore said to be mesoscopic when its size is in between the microscopic scale, set by the mean free path, and the macroscopic scale, set by the phase-coherence length, $l < L < L_\varphi$. A sample is therefore only self-averaging with respect to the impurity scattering for samples of size larger than the phase-coherence length.[51] A sample will therefore only exhibit the weak-localization effect when its size is much larger than the phase-coherence length but much smaller than the localization length $L_\varphi < L < \xi$.

An important way to reveal the conductance fluctuations experimentally is to measure the magnetoresistance of a given sample. To study the fluctuation effects in magnetic fields, we must study the dependence of the variance on the

[50] For example for a wire we have $g(L) = g(L_\varphi)\, L/L_\varphi$.

[51] The conductance entering the scaling theory of localization is thus assumed averaged over phase-incoherent volumes.

magnetic fields $\Delta G_{\alpha\beta}(\mathbf{B}_+, \mathbf{B}_-)$, where $\mathbf{B}_+$ is the sum and $\mathbf{B}_-$ the difference in the magnetic fields influencing the outer and inner loops. Since the conductance loops can correspond to samples placed in different field strengths, the diffusion pole appearing in a fluctuation diagram will not be immune to the presence of magnetic fields, as in the case when the Diffuson describes diffusion within a given sample, since particle conservation is, of course, unaffected by the presence of a magnetic field. According to the low-field prescription for inclusion of magnetic fields, eq.(11.29), we get for the Diffuson

$$D_0 \left\{ (-i\nabla_{\mathbf{x}} - \frac{e}{\hbar}\mathbf{A}_-(\mathbf{x}))^2 + 1/\tau_\varphi \right\} \tilde{D}(\mathbf{x}, \mathbf{x}') = \frac{1}{\tau}\delta(\mathbf{x} - \mathbf{x}') \tag{11.251}$$

where $\mathbf{A}_-$ is the vector potential corresponding to the difference in magnetic fields, $\mathbf{B}_- = \nabla_{\mathbf{x}} \times \mathbf{A}_-$, and we have introduced the phase-breaking rate in view of the above consideration. In the case of the Diffuson, the magnetic field induced phases subtract, accounting for the appearance of the difference of the vector potentials $\mathbf{A}_-$. For the case of the Cooperon, the two phases add, and we obtain

$$D_0 \left\{ (-i\nabla_{\mathbf{x}} - \frac{e}{\hbar}\mathbf{A}_+(\mathbf{x}))^2 + 1/\tau_\varphi \right\} \tilde{C}(\mathbf{x}, \mathbf{x}') = \frac{1}{\tau}\delta(\mathbf{x} - \mathbf{x}') \tag{11.252}$$

where $\mathbf{A}_+$ is the vector potential corresponding to the sum of the fields, $\mathbf{B}_+ = \nabla \times \mathbf{A}_+$.

The *magneto-fingerprint* of a given sample, i.e., the dependence of its conductance on an external magnetic will show an erratic pattern with a given peak to valley ratio and a correlation field strength B_c. This, however, is not immediately the information we obtain by calculating the variance

$$\Delta G_{\alpha\beta,\gamma\delta}(\mathbf{B}_+, \mathbf{B}_-) = < [G_{\alpha\beta}(\mathbf{B}_1) - < G_{\alpha\beta}(\mathbf{B}_1) >][G_{\gamma\delta}(\mathbf{B}_2) - < G_{\gamma\delta}(\mathbf{B}_2) >] > \tag{11.253}$$

where $\mathbf{B}_1$ is the field in, say, the inner loop, $\mathbf{B}_1 = (\mathbf{B}_+ + \mathbf{B}_-)/2$, and $\mathbf{B}_2$ is the field in the outer loop, $\mathbf{B}_2 = (\mathbf{B}_+ - \mathbf{B}_-)/2$. In the variance, the magnetic fields are fixed in the two samples, and we are averaging over different impurity configurations, thus describing a situation in which the actual impurity configuration is changed, a hardly controllable endeavor from an experimental point of view. However, if the magnetoconductance of a given sample, $G(B)$, varies randomly with magnetic field, the two types of averages – the one with respect to magnetic field and the one with respect to impurity configuration – are equivalent, and the characteristics of the magneto-fingerprint can be extracted from the correlation function in eq.(11.253). The physical reason for the validity of such an *ergodic* hypothesis [78], [79], that changing magnetic field is equivalent to changing impurity configuration is, that since the electronic motion in the sample is quantum mechanically coherent the wave function pattern is sensitive to the position of all the impurities in the sample, just as the presence of the magnetic field is felt throughout the sample by the electron.[52] The extreme sensitivity to impurity configuration is also witnessed by

[52]The validity of the ergodic hypothesis has been substantiated in reference [80].

the fact that changing the position of one impurity by an atomic distance, $1/k_F$, is equivalent to shifting all the impurities by arbitrary amounts, i.e., to create a completely different sample [81], [82].

The ergodic hypothesis can be elucidated by the following consideration. In the mean square of the probability for propagating between two points in space we encounter the correlation function

$$< \Big(\cos(\phi_c(B_1) - \phi_{c'}(B_1)) \Big) \Big(\cos(\phi_c(B_2) - \phi_{c'}(B_2)) \Big) >_{imp} \tag{11.254}$$

where $(\phi_c(B) - \phi_{c'}(B))$ depends on the phases picked up due to the magnetic field, i.e., the flux through the area enclosed by the trajectories c and c'. When the magnetic field B_1 changes its value to B_2 (where the correlation function equals one half), the phase factor changes by 2π times the flux through the area enclosed by the trajectories c and c' in units of the flux quantum. This change, however, is equivalent to what happens when changing to a different impurity configuration for fixed magnetic field, i.e., the quantity we calculate.[53]

In order to calculate the variance in eq.(11.253) we must solve eq.(11.251) and eq.(11.252) with the appropriate mixed boundary value conditions in the presence of magnetic fields, and insert the solutions into contributions like that in eq.(11.240). However, determination of the characteristic correlations of the aperiodic magnetoconductance fluctuations can be done by inspection of eq.(11.251) and eq.(11.252). The correlation field B_c is determined by the sample-to-sample change in the magnetic field, i.e., $\mathbf{B}_-$. According to eq.(11.251) and eq.(11.252), this field is determined either by the sample size, through the gradient term, or the phase coherence length. When the phase-coherence length is longer than the sample size, the correlation field is therefore of order of the flux quantum divided by the sample area, $B_c \sim \phi_0/L^2$, where ϕ_0 is the normal flux quantum $\phi_0 = 2\pi\hbar/|e|$, since the typical diffusion loops, like those depicted in figures 11.6 and 11.7 enclose an area of the order of the sample, L^2. We note that in magnetic fields exceeding $\max\{\phi_0/L^2, \phi_0/L_\varphi^2\}$, the Cooperon no longer contributes to the field dependence of the conductance fluctuations, because its dependence on magnetic field is suppressed according to the weak-localization analysis.[54]

We note that the weak-localization and mesoscopic fluctuation phenomena are a general feature of wave propagation in a random media, be the wave nature classical, such as sound and light,[55] or of quantum origin such as for the motion of electrons. The weak-localization effect was in fact originally envisaged for the multiple scattering of electromagnetic waves [42]. The coherent backscattering effect has been studied experimentally for light waves (for a review on classical wave propagation in random media, see reference [84]). For the wealth of interesting

[53]Another way of revealing the mesoscopic fluctuations is to change the Fermi energy (i.e., the density of conduction electron as is feasible in an inversion layer). The typical energy scale E_c for these fluctuations is analogously determined by the typical time τ_{trav} it takes an electron to traverse the sample according to $E_c \sim \hbar/\tau_{trav}$. In the diffusive regime we have $\tau_{trav} \sim L^2/D_0$.

[54]For an account of the experimental discovery of conductance fluctuations, see reference [83].

[55]Here we refer to conditions described by Maxwell's equations.

weak-localization and mesoscopic fluctuation effects, we refer to the references cited in for example the references [58], [59], [70], [83], [85], [86], [87], [88].

Appendix A

Path Integrals and Propagators

In classical mechanics only the classical paths are of physical relevance; however, stating the quantum law of motion involved all paths. The way in which the various alternative paths contribute to the expression for the propagator was realized by Dirac [89], who noted that the conditional amplitude for an infinitesimal time step is related to Lagrange's function, L, according to

$$<\mathbf{x}, t+\Delta t|\mathbf{x}', t> \propto e^{\frac{i}{\hbar}\Delta t\, L(\mathbf{x},(\mathbf{x}-\mathbf{x}')/\Delta t)} \tag{A.1}$$

however, with L expressed in terms of the coordinates at time t and $t+\Delta t$. This gem of Dirac's was turned into brilliance by Feynman, and provided the intuitive approach to quantum mechanics as described in section 1.1. We shall here obtain the path integral expression for Dirac's transformation function $<\mathbf{x}, t|\mathbf{x}', t'>$.

Propagating in small steps by inserting complete sets at intermediate times we have for the propagator

$$\begin{aligned} <\mathbf{x}, t|\mathbf{x}', t'> &= \int d\mathbf{x}_1 \int d\mathbf{x}_2 .. \int d\mathbf{x}_N \; <\mathbf{x}, t|\mathbf{x}_N, t_N><\mathbf{x}_N, t_N|\mathbf{x}_{N-1}, t_{N-1}> \\ &\quad <\mathbf{x}_{N-1}, t_{N-1}|\mathbf{x}_{N-2}, t_{N-2}> .. <\mathbf{x}_1, t_1|\mathbf{x}', t'> \; . \end{aligned} \tag{A.2}$$

We are consequently interested in the transformation function for infinitesimal times, and from eq.(1.97) we obtain

$$\begin{aligned} <\mathbf{x}_n, t_n|\mathbf{x}_{n-1}, t_{n-1}> &= <\mathbf{x}_n|e^{-\frac{i}{\hbar}\Delta t\hat{H}(t_n)}|\mathbf{x}_{n-1}> \\ &= \delta(\mathbf{x}_n - \mathbf{x}_{n-1}) + \frac{\Delta t}{i\hbar} <\mathbf{x}_n|\hat{H}(t_n)|\mathbf{x}_{n-1}> \; + \mathcal{O}(\Delta t^2) \end{aligned} \tag{A.3}$$

where $\Delta t = t_n - t_{n-1} = (t-t')/(N+1))$, as we have inserted N intermediate resolutions of the identity.

In the following we shall consider a particle of mass m in a potential V for which we have the Hamiltonian

$$\hat{H}(t) = \frac{\hat{\mathbf{p}}^2}{2m} + V(\hat{\mathbf{x}}, t) \; . \tag{A.4}$$